

A European Daily High-resolution Observational Gridded Data set of Sea Level Pressure

E. J. M. van den Besselaar¹, M. R. Haylock², G. van der Schrier¹, and A. M.

G. Klein Tank¹

E. J. M. van den Besselaar, Royal Netherlands Meteorological Institute, PO Box 201, 3730 AE
De Bilt, The Netherlands

M.R. Haylock, PartnerRe, Bellerivestrasse 36, 8034 Zurich, Switzerland

A. M. G. Klein Tank, Royal Netherlands Meteorological Institute, PO Box 201, 3730 AE De
Bilt, The Netherlands

G. van der Schrier, Royal Netherlands Meteorological Institute, PO Box 201, 3730 AE De Bilt,
The Netherlands

¹Royal Netherlands Meteorological
Institute (KNMI), De Bilt, The Netherlands

²PartnerRe, Zurich, Switzerland

Abstract. In this study we introduce a daily high-resolution land-only observational gridded data set for sea level pressure covering the European region as a new addition to the E-OBS gridded data sets of daily temperatures and precipitation amounts. This data set improves upon existing products in terms of spatial resolution and extent. The data set is delivered on the same four spatial resolutions as the other E-OBS data sets; 0.25° by 0.25° and 0.5° by 0.5° on a regular latitude-longitude grid, and 0.22° by 0.22° and 0.44° by 0.44° on a rotated pole grid. We show that there is a good agreement in the long term mean and standard deviation with popular reanalysis grids. In areas with a relatively high number of stations, the gridded data is closer to the station data than the reanalysis products. There is also a very good agreement with daily weather charts for selected storm events.

1. Introduction

Interpolating observational data sets to a regular grid is important for climate research as the meteorological stations are irregularly spaced. These gridded data sets allow best estimates of climate variables at locations away from observing stations and therefore allow studying climate in data sparse regions.

Studies of climate change are often limited to temperature and precipitation changes, but there is a question as to whether human influence is detectable in other variables as well. For example, Gillett et al [2003] detected an influence of anthropogenic greenhouse gases and sulphate aerosols in observations of winter sea level pressure (December to February), using combined simulations from four climate models. However, in their study they noted the substantial underestimation of the magnitude of the sea level pressure response in these models. This suggests that variations in climate model simulations of the large-scale circulation may be too small, which points to the importance of observational data sets for sea level pressure. Also, sea level pressure variability and related storminess indices are important in climate change studies [Barring and von Storch, 2004; Hanna et al, 2008; Wang et al, 2009].

In this paper we present a European daily high-resolution land-only data set of sea level pressure. This data set is provided as a new part of the E-OBS gridded data set which currently consists of precipitation and temperature (minimum, mean and maximum) [Haylock et al, 2008].

Several sea level pressure gridded data sets are currently available, but they have either a coarser resolution [e.g. 5° by 5° using only 86 land and island stations; Ansell et al, 2006]

or smaller spatial and/or temporal scale [e.g. monthly data sets for UK only; Perry and Hollis, 2005] than the one presented here. Other gridded data sets for sea level pressure are reanalysis data, such as ERA40/ERA-interim [Uppala et al, 2005], NCEP/NCAR [Kalnay et al, 1996] and NOAA-CIRES 20th Century Reanalysis [Compo et al, 2011, 2006]. Also, none of the existing observational data sets includes error estimates.

The data and method used to create the E-OBS sea level pressure grid are presented in Sect. 2. Comparisons with reanalysis data and weather charts are given in Sect. 3 and we end with a conclusion in Sect. 4.

2. Data & Method

2.1. Data Collection & Quality

The data used for the gridding comes from the European Climate Assessment and Data set (ECA&D; <http://eca.knmi.nl>) [Klein Tank et al, 2002; Klok and Klein Tank, 2008] for the time period 1950 to present. ECA&D is collecting station observations from currently 12 elements of over 3500 stations and is gradually expanding. These station observations are all received as daily values. Currently (October 2010), 416 of the available stations have sea level pressure series available with 147 stations having long series for at least 50 years. The location of all stations are shown in Fig. 1 and the number of pressure stations used over time in Fig. 2. The number of pressure stations is much less than the number of temperature or precipitation stations ($\sim 1500 - 3000$ stations, respectively). However, sea level pressure is expected to be more spatially homogeneous over the area so that the number of stations needed for the gridding procedure can be less than those needed for other elements.

The use of sea level pressure from a rather sparse network means that small-scale pressure systems are not captured in this data set. This handicap is obviously more severe for the sparsely sampled countries like France where the characteristic distance between stations that provide sea level pressure is ~ 450 km, than for countries with a high station density like the Netherlands where this typical distance is an order of magnitude smaller at ~ 40 km.

Using daily averaged sea level pressure prevents a reconstruction of e.g. moving frontal structures or secondary lows behind a moving cold front. More general: if the typical length-scale of phenomena is much smaller than the distance these phenomena cover in a day, then the temporal resolution of the data set makes that these phenomena are not captured in the E-OBS data set.

There are several different measuring intervals used by the ECA&D data providers for providing the daily values. One country determines daily mean pressure between 0-0 UT while another country determines it between 18-18 UT or even at other times. If this was the case, we made sure that the date on which the value was recorded in our time series corresponds to the day that includes the longest part of the measuring interval. For example, if a daily value was determined from 7 UT on 1 January 1950 to 7 UT on 2 January 1950, the data provider might have recorded this value on 2 January 1950. The longest part of this measuring interval falls actually on 1 January 1950 and therefore we have shifted this value to 1 January 1950 to have the best estimate for the daily value on 1 January 1950. Omitting this date shift will result in areas within the gridded pressure data set which will be more representative for the next day. The data quality will thus

improve by this procedure. This shift was needed for less than 1% of the available pressure series.

Most of these series were received as daily mean sea level pressure series. The methods used by the data providers to correct the station level pressure series to sea level pressure are unknown to ECA&D staff. Series from 112 stations in Serbia, Slovenia, Estonia, Croatia, Czech Republic and Slovakia were received as daily mean station level pressure. These series were corrected to sea level pressure using hydrostatic balance and the equation of state, which are integrated from sea level to the height of the station. This gives

$$p_0 = p_z e^{\left(\frac{zg}{RT}\right)}, \quad (1)$$

where p_0 is daily mean sea level pressure, p_z daily mean pressure at station level, z station elevation (which we assume to be equal to the barometer altitude), g Earth's gravity (9.80665 m s^{-2}), R the gas constant for dry air ($287.058 \text{ J kg}^{-1} \text{ K}^{-1}$) and T the daily mean temperature of that station in Kelvin. Note that the simplification is made of assuming that the column of air from station level to sea level is uniform at temperature T . In reality this will not be the case and the temperature will decrease with height. This means that ECA&D slightly overestimates the sea level pressure when this approach is used. As we have used a very simple model here, this bias might be seen as an upper limit of the bias of the unknown methods used by the data providers to correct station level pressure to sea level pressure. This slight bias is not included in the interpolation error.

Assuming hydrostatic equilibrium in the atmosphere, $\partial p / \partial z = -\rho g$, the pressure at a given level z is

$$p(z) = \int_z^\infty \rho dz. \quad (2)$$

Substituting the equation of state for ρ in the hydrostatic equation gives:

$$\frac{dp}{p} = -\frac{gdz}{R_d T} \quad (3)$$

where T is the in situ temperature at height z (actually, it is the virtual temperature [Peixoto and Oort, 1992, §3.5.1]). Integration of this equation from $z = 0$ to the level z then gives:

$$p(z) = p_0 e^{-\int_0^z g/(R_d T) dz}. \quad (4)$$

The in situ temperature at height z can be related to the temperature T_s at station level using vapor pressure e and air pressure p , but this requires knowledge on the vapor pressure which is not available. A simplification is introduced here, assuming a constant lapse rate λ of -0.6°C per 100 m. The in situ temperature at height z is then given by:

$$T(z) = T_s - z\lambda \quad (5)$$

Substituting (5) into (4) gives:

$$p(z) = p_0 e^{-\int_0^z g/(R_d(T+\lambda z)) dz}. \quad (6)$$

For an isothermal layer, $\lambda = 0$, integration of Eq. (6) gives Eq. (1), the ECA&D assumption. Otherwise, this integral gives:

$$p(z) = p_0 e^{(g/R_d \lambda)[\ln(R_d \lambda z + R_d T) - \ln(R_d T)]}. \quad (7)$$

Both values of sea level pressure have been calculated for station elevations from 0 to 1000 m and station temperatures from -10 to 30°C . Figure 3 gives the difference between the sea level pressure as calculated from Eq. (7) minus that from Eq. (1). The overestimation in ECA&D is highest for high elevations and low daily average temperatures, and only for the 112 stations for which the series were corrected by ECA&D. A histogram of

the elevations of these stations is shown in Fig. 4. The majority of these stations have an elevation not exceeding 500 m.

The available validated time series usually do not extend to the present time. Therefore unvalidated synoptical messages sent by the Global Telecommunication System (GTS) [WMO, 2007] are used for the most recent time period when validated data series are not yet available. Furthermore, possible gaps in the series are filled in with nearby stations as long as these are less than 25 km away and have less than 50 m height difference [Klein Tank et al, 2002; ECA&D Project team, 2010]. The resulting blended station series are used in the gridding procedure.

Basic quality control is performed on the sea level pressure series. If the daily mean sea level pressure is below 900 hPa, above 1080 hPa or repetitive (i.e. exactly the same) for 5 days or more in a row, that day is flagged as suspect and not used in the gridding procedures [ECA&D Project team, 2010]. At present no attempts are made to correct suspect data. Currently, no homogeneity checks or corrections are made for pressure data in the gridded data set. About 75% of the stations that have 80% non-missing sea level pressure data for the period 1950-2010 are classified as useful. The inhomogeneous stations are mainly located in Spain and the Balkan Peninsula. Homogeneity checks for all E-OBS grids will be part of a future version of E-OBS.

2.2. Gridding Procedure

Several interpolation methods are compared for temperature, precipitation and sea level pressure by Hofstra et al [2008]. Their analysis concludes that the method which involves kriging using a geographically-independent variogram is the best interpolation method for the E-OBS data set for all currently used parameters including sea level pressure. The

gridding procedures are described in detail by Haylock et al [2008], therefore we only give a brief summary here.

Kriging involves solving a set of linear equations to minimize the variance of the observations around the interpolating surface. This least squares problem therefore assumes that the station data being interpolated are homogeneous in space. This is not the case when we have stations across Europe from many climate zones. The daily data therefore need to be made homogeneous across the region.

This problem was addressed by adopting a three-step methodology of interpolating the daily data: interpolating the monthly mean using thin-plate splines to define the underlying spatial structure of the data; kriging the daily anomalies with regard to the monthly mean; and applying the interpolated daily anomaly to the interpolated monthly mean to create the final result. This is similar to universal kriging [Journel and Huijbregts, 1978], where a polynomial is fit to the underlying spatial trend. In such a large and complex region as Europe, thin-plate splines are a more appropriate method for trend estimation than polynomials. For monthly mean sea level pressure we used two-dimensional splines as sea level pressure is not dependent on station elevation.

The observations were first interpolated to a high-resolution 0.1° by 0.1° rotated pole mastergrid, with the “North Pole” at 162°W , 39.25°N . A rotated pole grid was chosen so as to allow quasi-equal area grid spacing over the European region. This enabled the largest spatial coverage with the minimum number of interpolated grid squares to increase computational efficiency. Using an unrotated grid would have resulted in a higher grid density in the north of the region compared to the south. The rotated pole was chosen to match the grid used by many of the RCMs used in, for example, the ENSEMBLES

project [van der Linden and Mitchell, 2009, and references therein]. This mastergrid was then averaged to produce 0.22° by 0.22° and 0.44° by 0.44° rotated pole grids, and 0.25° by 0.25° and 0.5° by 0.5° regular latitude-longitude grids. The period used is 1950 to the present. The grid is calculated for the region from -35 to 25°E and from -23.4 to 23.6°N in the rotated pole grid. This corresponds to about -30 to 55°E and 25 to 75°N in the regular latitude-longitude grid. Grid boxes without valid data and sea grid boxes are indicated with missing values.

The E-OBS gridded data set also includes an estimate of the interpolation uncertainty. For the monthly uncertainty, we used the uncertainty determined by interpolating the monthly climatology (from all available years) and applied this to all years because of computational constraints. The method of addressing uncertainty is based on the premise that we would expect higher uncertainty at an interpolated point when the neighbors are more variable. When neighbors are similar, one would expect less uncertainty. We applied the method of Yamamoto [2000] to every grid point for every day to arrive at the standard error for the daily anomaly. The final uncertainty at a grid point was calculated by combining the uncertainties from the monthly climatology and the daily anomaly in quadrature, i.e., the square root of the sum of the squares of the two uncertainties. For more information on the calculation of the uncertainties, we refer to Haylock et al [2008].

3. Comparison With Other Data Sets

3.1. Reanalysis Data Sets

To check the results of our gridding procedure, we compared our gridded data set with other existing data sets. The only data sets with a spatial coverage that matches ours are reanalysis products. The reanalysis sea level pressure grids cover at least the European

area and have a resolution between 1.5° by 1.5° and 2.5° by 2.5° . As this resolution is still considerably coarser than the ones for the E-OBS grid, we averaged our 0.1° by 0.1° mastergrid to the same resolution as each of the reanalysis grids.

The ERA-40, ERA-interim [Uppala et al, 2005] and 20th Century Reanalysis version 2 grids [Compo et al, 2011, 2006] are available as four times per day (00, 06, 12, 18 UTC). These four daily values were averaged to compute daily means. The NCEP/NCAR grid [Kalnay et al, 1996] was already available as daily means. For the 20th Century Reanalysis we used the ensemble mean.

Motivated by the fact that the common period of these data sets is from 1 January 1989 to 31 December 2001, we limit the comparison between the E-OBS sea level pressure grid and the reanalysis grids to this period only. Using different periods in comparing the E-OBS sea level pressure grid and the reanalysis grids will influence the results of the comparisons since the lengths of these periods are vastly different.

In Fig. 5 the comparisons between the E-OBS sea level pressure grid and the reanalysis grids are shown. ERA-40 shows the same behavior as ERA-interim, although on a coarser grid than ERA-interim. Therefore, only the comparison with ERA-interim is shown. For each grid box, the mean and standard deviation of the daily averaged maps over the chosen time period are determined. Then the grid box differences in the mean and standard deviation are taken between the E-OBS grid box and the corresponding reanalysis grid box when both data sets have non-missing data. These differences are shown in Fig. 5. The left column shows the difference in the mean and the right column the difference in the standard deviation. The top row shows the comparison with NCEP/NCAR, the middle row with ERA-interim and the bottom show the comparison with the 20th Century

Reanalysis. Note that the color range for the bottom left panel (20th Century Reanalysis) is much larger than for the other panels (-4 to 4 hPa instead of -1.5 to 1.5 hPa).

Figure 5 shows that NCEP/NCAR and ERA-interim show generally the same behavior for the mean pressure field. Central Europe has higher mean pressure for the E-OBS grid than for the reanalysis fields, while in other parts the pressure in the E-OBS grids is slightly lower than for the reanalysis fields. The 20th Century Reanalysis has an overall much higher mean pressure than E-OBS, up to 4 hPa or higher in large areas.

The panels for standard deviation show how the variations in time are captured. It is seen that E-OBS has much larger variation compared to both the 20th Century Reanalysis and ERA-interim, although ERA-interim still has more variation than the 20th Century Reanalysis. E-OBS and NCEP/NCAR have about the same variations in their fields. This indicates that NCEP/NCAR is better in capturing pressure extremes in the observed day-to-day pressure fields than the other reanalysis grids.

The E-OBS data set also makes the interpolation uncertainty available. This uncertainty for the period 1989–2001 using E-OBS, regridded onto the NCEP/NCAR grid, is shown in Fig. 6. Variations in the *averaged* interpolation error are very small, from 0.136 to 0.144 hPa. Lower values are seen over a broad band stretching from the Balkan Peninsula to northwestern Europe and coincide with areas where station density is high (Fig. 1). Higher values of the interpolation error are seen outside this band, particularly the Iberian Peninsula, most of France, southeastern Europe and northern Scandinavia, coinciding with areas where the station density is low. Although there are rough similarities between Fig. 6 and the upper left figure of Fig. 5, the amplitudes shown are an order of magnitude apart. Furthermore, the pattern in Fig. 6 does not resemble the pattern of the upper right

figure of Fig. 5. This indicates that the differences between E-OBS and NCEP/NCAR (and other data sets used here) are not due to variations in the station density used for the E-OBS grid alone.

The same comparison has been done for the winter period (DJF) and summer period (JJA). The standard deviation for NCEP/NCAR in winter and summer is shown in Fig. 7. While the yearly variation in NCEP/NCAR is about the same as in E-OBS (top right panel of Fig. 5), the variation in winter is less than in E-OBS and in summer it is slightly larger. For ERA-interim and 20th Century Reanalysis the variation is lower than E-OBS in both winter and summer.

This shows that E-OBS verifies very well with the NCEP/NCAR and ERA data sets, and that much of the day-to-day variability in sea level pressure is present in the gridded data set, matching existing reanalysis products in this respect.

In order to explain the observed differences between the E-OBS and reanalysis sea level pressure products, we show in Fig. 8 the sea level pressure time series for three grid boxes in the NCEP/NCAR data set together with the same grid box in the E-OBS data set regridded onto the NCEP/NCAR grid. Station data of one station located in the grid box is added as a third element. For this comparison the NCEP/NCAR data set was chosen as this one shows the best agreement with the E-OBS data set. We chose only one station present in a grid box as a reference. Since the de-correlation length scale of sea level pressure is an order of magnitude larger than the grid size used, daily fields of sea level pressure are spatially sufficiently homogeneous to take data from one station as representative for the grid box. Here we show daily data for 1990 as an example.

The differences between the grid box time series and station time series are shown in the lower part of each panel. The top panel shows the grid box located over the Netherlands. The station density is high in this area with 22 stations in that grid box (13 covering 1989–2001). The middle one shows the grid box located over Southern Norway with 13 stations in the grid box (5 covering 1989–2001). The grid box located over Western Spain is shown in the bottom panel with only 2 stations in that grid box (both covering 1989–2001). From the difference plots, it is clear that a higher station density results in E-OBS grid box values resembling more closely the station time series. A simple conceptual model to explain this is to view station observations as the sum of the true grid box mean and an error term. A higher station density leads to a better estimate of the true grid box mean, which minimizes the expected difference between the estimate and the station observations. For NCEP/NCAR the differences with the station data are about the same in all three grid boxes, with up to 5 hPa difference on some days.

Inhomogeneities in the station series might interfere with a comparison as shown in Fig. 8. The homogeneity test results from the ECA&D website indicate that the stations near the grid boxes in Norway and the Netherlands are considered homogeneous. The stations in Spain within the grid box of this example (Salamanca Aeropuerto and Navacerrata) are homogeneous for the period 1961–2010 (there is not enough data to determine the homogeneity tests over the period 1950–2010). Madrid Retiro (located further away and thus weakly influencing the value of this particular grid box) is marked as inhomogeneous for the period 1950–2010, but the break is detected in the year 1993; outside the interval shown in this example.

3.2. Weather Charts

Daily sea level pressure grids and selected weather charts are compared to assess the ability of E-OBS in reproducing individual storms. The weather charts are the output of weather forecast models with sometimes a correction made by the forecast meteorologist when needed. The charts shown here were made 6 hours before the time the chart was valid, e.g. a chart of 12 UTC was produced at 06 UTC. Two prominent storm events are highlighted here; the Christmas storms of 1999 [see e.g. Buizza and Hollingsworth, 2002] and Xynthia of 28 February 2010 [see e.g. Kolen et al, 2010].

We have chosen the Christmas storms of 1999 as this time period is also included in the comparison with the reanalysis grids. The top panel of Fig. 9 shows the weather chart of 24 December 1999 at 12 UTC from the Royal Netherlands Meteorological Institute (KNMI). The weather chart of 25 December 1999 at 00 UTC from <http://www.wetterzentrale.de> is shown in the middle panel. The daily mean sea level pressure for 24 December 1999 from the E-OBS grid is shown in the bottom panel. The isobars are shown as thin lines in the E-OBS grid while the pressure values themselves are shown with colors. There are some differences which we would expect as the weather charts are for specific times, while the E-OBS grid shows daily mean pressure. However, the overall agreement is very good. The isobars in the gridded data set and the weather charts are aligned and have the same values. The weather charts show a low pressure region to the north of Scotland over the Atlantic ocean. The E-OBS grid is a land-only grid, so the center of the low pressure region is not captured. However, the pressure in E-OBS decreases toward the region north of Scotland, correctly indicating the position of the low pressure region.

Next to 24 December 1999 we have also compared the weather charts of 25 and 26 December 1999 with the E-OBS sea level pressure grids (not shown). These comparisons

also give a very good agreement between the E-OBS sea level pressure grid and the weather charts.

The comparison between weather charts and E-OBS of the more recent storm Xynthia of 28 February 2010 is shown in Fig. 10. The top four panels show the weather charts of 28 February 2010 at 00, 06, 12 and 18 UTC and the bottom panel shows the E-OBS grid for 28 February 2010. On the 12 UTC chart the center of the storm is located near the Netherlands, around the center of the track of the storm followed during this day. This is captured by the daily E-OBS grid as well, showing also in this case a very good agreement with the weather chart.

The bottom panels of Figs. 9 and 10 show an unrealistically strong gradient in Southeast Europe. We relate this feature to a low station density in that region resulting in a situation where remote stations influence the gridded sea level pressure values over vast areas. This confirms the observation of Fig. 8 that high station density results in the E-OBS grid box values resembling more closely the observed station time series.

4. Conclusion

In this paper we introduced a land-only daily mean sea level pressure grid covering a large part of Europe as a new addition to the E-OBS gridded data sets. It is compiled from station sea level pressure series available in ECA&D for the period 1950 to present. This data set is compared with available reanalysis data sets and differences in the long-term mean and standard deviation were studied. The E-OBS grid shows a good agreement with the NCEP/NCAR reanalysis grid, but a lower agreement with the ERA-40, ERA-interim and 20th Century Reanalysis version 2 grids. On a daily basis the E-OBS grids were compared with weather charts around the time of the Christmas storms in 1999 and the

more recent storm Xynthia in 2010. Although the weather charts are for specific times while the E-OBS grids are daily means, there is still a very good agreement. Therefore we conclude that this new sea level pressure grid is suitable for several research areas, such as monitoring climate change or comparisons with Regional Climate Models. This study again confirms that the quality of the E-OBS gridded data is depending on the station density. We hope to increase the station density of sea level pressure stations in ECA&D in the future, thereby improving the E-OBS gridded data set, especially in terms of capturing weather patterns such as storms.

Acknowledgments. We acknowledge the data providers in the ECA&D project (<http://eca.knmi.nl>). ECMWF ERA-40 and ERA interim data used in this study have been obtained from the ECMWF data server. NCEP/NCAR Reanalysis data and 20th Century Reanalysis data provided by the NOAA/OAR/ESRL PSD, Boulder, Colorado, USA, from their Web site at <http://www.esrl.noaa.gov/psd>.

References

Ansell T, Jones P, Allen R, Lister D, Parker D, Brunet M, Moberg A, Jacobeitt J, Brohan P, Rayner N, Aguilar E, Alexandersson H, Barriendos M, Brandsma T, Cox N, Della-Marta P, Drebs A, Founda D, Gerstengarbe F, Hickey K, Jónsson T, Luterbacher J, Nordli Ø, Oesterle H, Petrakis M, Philipp A, Rodwell M, Saladie O, Sigro J, Slonosky V, Srnec L, Swail V, García-Suárez A, Tuomenvirta H, Wang X, Wanner H, Werner P, Wheeler D, Xoplaki E (2006) Daily mean sea level pressure reconstruction for the European-North Atlantic region for the period 1850-2003. *J Climate* 19:2717–2742

- Barring L, von Storch H (2004) Northern European Storminess since about 1800. *Geophys Res Lett* 31:L20,202, doi:10.1029/2004GL020441
- Buizza R, Hollingsworth A (2002) Storm prediction over Europe using the ECMWF Ensemble Prediction System. *Meteor Appl* 9:289–305, doi:10.1017/S1350482702003031
- Compo G, Whitaker J, Sardeshmukh P (2006) Feasibility of a 100 year reanalysis using only surface pressure data. *Bull Amer Meteor Soc* 87:175–190
- Compo G, Whitaker J, Sardeshmukh P, Matsui N, Allan R, Yin X, Gleason B, Vose R, Rutledge G, Bessemoulin P, Brönnimann S, Brunet M, Crouthamel R, Grant A, Groisman P, Jones P, Kruk M, Kruger A, Marshall G, Maugeri M, Mok H, Nordli Ø, Ross T, Trigo R, Wang X, Woodruff S, Worley S (2011) The Twentieth Century Reanalysis Project. *Quart J Roy Meteor Soc* 137:1–28, doi:10.1002/qj.776
- ECA&D Project team (2010) Algorithm Theoretical Basis Document (ATBD). <http://eca.knmi.nl/documents/atbd.pdf>
- Gillett N, Zwiers F, Weaver A, Stott PA (2003) Detection of human influence on sea-level pressure. *Nature* 422:292–294, doi:10.1038/nature01487
- Hanna E, Capellen J, Allan R, Jónsson T, Le Blancq F, Lillington T, Hickey K (2008) New insights into Northern European and North Atlantic Surface Pressure Variability, Storminess, and Related Climatic Change since 1830. *J Climate* 21:6739–6766, doi:10.1175/2008JCLI2296.1
- Haylock M, Hofstra N, Tank AK, Klok E, Jones P, New M (2008) A European daily high-resolution gridded data set of surface temperature and precipitation for 1950-2006. *J Geophys Res* 113:D20,119, doi:10.1029/2008JD010201

Hofstra N, Haylock M, New M, Jones P, Frei C (2008) Comparison of six methods for the interpolation of daily, European climate data. *J Geophys Res* 113:D21,110, doi:10.1029/2008JD010100

Journel A, Huijbregts C (1978) *Mining Geostatistics*. 600 pp., Academic, London

Kalnay E, Kanamitsu M, Kistler R, Collins W, Deaven D, Gandin L, Iredell M, Saha S, White G, Woollen J, Zhu Y, Leetmaa A, Reynolds R, Chelliah M, Ebisuzaki W, Higgins W, Janowiak J, Mo KC, Ropelewski C, Wang J, Jenne R, Joseph D (1996) The NCEP/NCAR 40-year reanalysis project. *Bull Amer Meteor Soc* 77:437–470

Klein Tank A, Wijngaard J, Können G, Böhm R, Demarée G, Gocheva A, Mileta M, Pashiardis S, Hejkrlik L, Kern-Hansen C, Heino R, Bessemoulin P, Müller-Westermeier G, Tzanakou M, Szalai S, Pálsdóttir T, Fitzgerald D, Rubin S, Capaldo M, Maugeri M, Leitass A, Bukantis A, Aberfeld R, van Engelen A, Forland E, Mietus M, Coelho F, Mares C, Razuvaev V, Nieplova E, Cegnar T, Antonio López J, Dahlström B, Moberg A, Kirchhofer W, Ceylan A, Pachaliuk O, Alexander L, Petrovic P (2002) Daily dataset of 20th-century surface air temperature and precipitation series for the European Climate Assessment. *Int J Climatol* 22:1441–1453

Klok E, Klein Tank A (2008) Short communication: Updated and extended European dataset of daily climate observations. *Int J Climatol* DOI: 10.1002/joc.1779

Kolen B, Slomp R, van Balen W, Terpstra T, Bottema M, Nieuwenhuis S (2010) Learning from French experiences with storm Xynthia: Damages after a flood. *HKV LIJN IN WATER* and Rijkswaterstaat, Waterdienst

Peixoto J, Oort A (1992) *Physics of Climate*. American Institute of Physics, New York

Figure 1. Locations of stations with sea level pressure series.

Figure 2. Number of stations with sea level pressure series over time.

Perry M, Hollis D (2005) The generation of monthly gridded datasets for a range of climate variables over the UK. *Int J Climatol* 25:1041–1054, doi:10.1002/joc.1161

Uppala S, Kållberg P, Simmons A, Andrae U, da Costa Bechtold V, Fiorino M, Gibson J, Haseler J, Hernandez A, Kelly G, Li X, Onogi K, Saarinen S, Sokka N, Allan R, Andersson E, Arpe K, Balmaseda M, Beljaars A, van de Berg L, Bidlot J, Bormann N, Caires S, Chevallier F, Dethof A, Dragosavac M, Fisher M, Fuentes M, Hagemann S, Hólm E, Hoskins B, Isaksen L, Janssen P, Jenne R, McNally A, Mahfouf JF, Morcrette JJ, Rayner N, Saunders R, Simon P, Sterl A, Trenberth K, Untch A, Vasiljevic D, Viterbo P, Woollen J (2005) The ERA-40 re-analysis. *Quart J Roy Meteor Soc* 131:2961–3012, doi:10.1256/qj.04.176

van der Linden P, Mitchell J (eds) (2009) *ENSEMBLES: Climate Change and its Impacts: Summary of research and results from the ENSEMBLES project*. Met Office Hadley Centre, FitzRoy Road, Exeter, UK, 160pp.

Wang X, Zwiers F, Swail V, Feng Y (2009) Trends and variability of storminess in the Northeast Atlantic region, 1874–2007. *Clim Dynam* 33:1179–1195, doi:10.1007/s00382-008-0504-5

WMO (2007) *Manual on the Global Telecommunication System*. WMO–No. 386

Yamamoto J (2000) An alternative measure of the reliability of ordinary kriging estimates. *Math Geol* 32:489–509, doi:10.1023/A:1007577916868

Figure 3. Difference in pressure between constant lapse rate and the ECA&D assumption. From bottom to top: Solid line for -10°C , dashed for 0°C , dashed-dotted for 10°C , dotted for 20°C and dash-dot-dot-dot for 30°C .

Figure 4. Histogram of the 112 stations for which the series were corrected to sea level by ECA&D.

Figure 5. Difference in sea level pressure between E-OBS and NCEP/NCAR (top row), ERA-interim (middle row) and NOAA-CIRES 20th Century Reanalysis version 2 (bottom row) for the period 1989-2001. Left: mean of the series. Right: standard deviation of the series. Please note the adjusted color range for the bottom left panel.

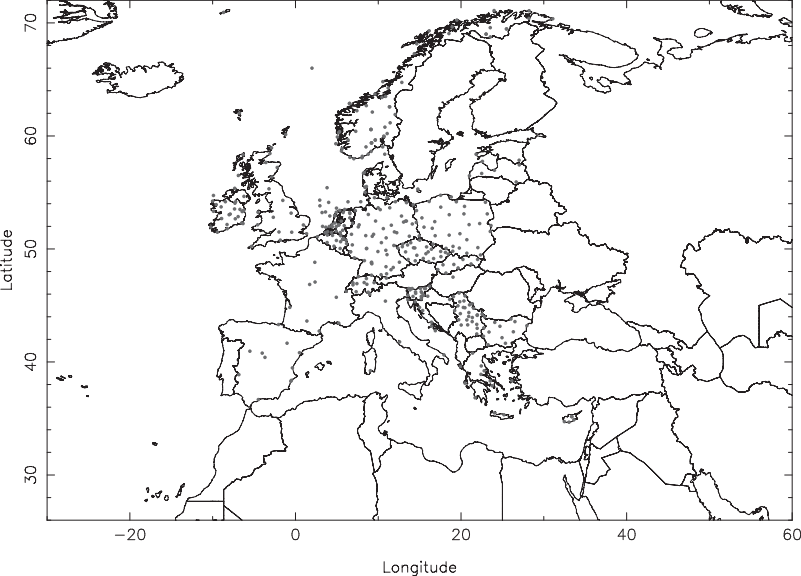
Figure 6. E-OBS uncertainty using NCEP/NCAR grid resolution for the period 1989-2001.

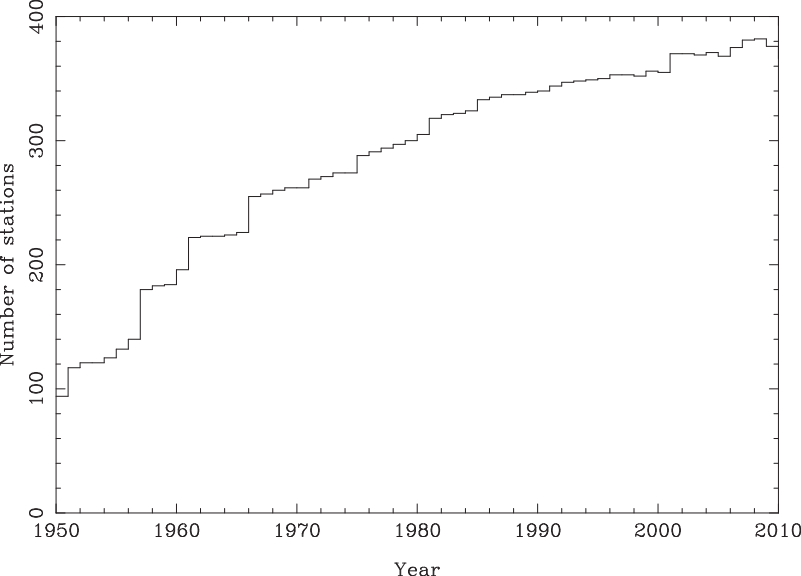
Figure 7. Difference in standard deviation between E-OBS sea level pressure and NCEP/NCAR. Left: winter. Right: summer.

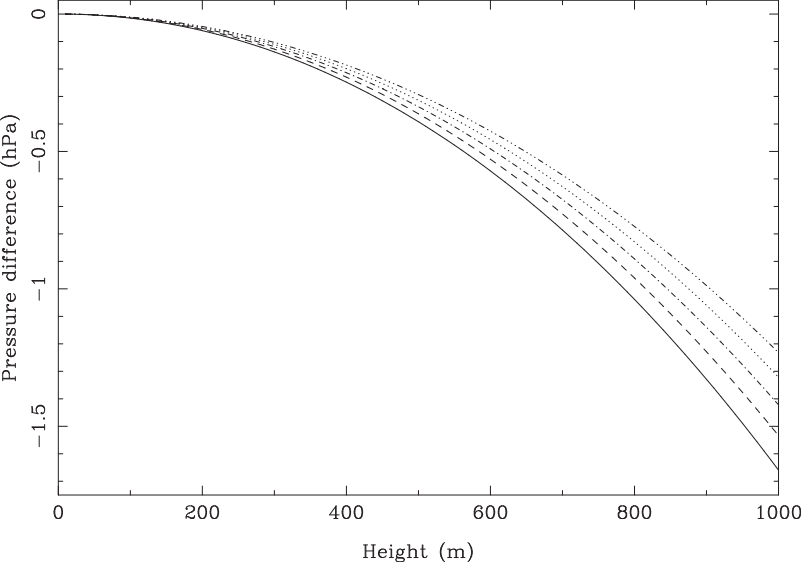
Figure 8. Time series for E-OBS (red), NCEP/NCAR (green) and one station (black) for three different grid boxes together with the differences between the grid box and station time series. Top: grid box located over the Netherlands, station De Bilt is used out of 22 station in that box. Middle: grid box located over Southern Norway, station Oslo Blindern is used out of 13 stations. Bottom: grid box located over Western Spain, station Salamanca Airport is used out of 2 stations.

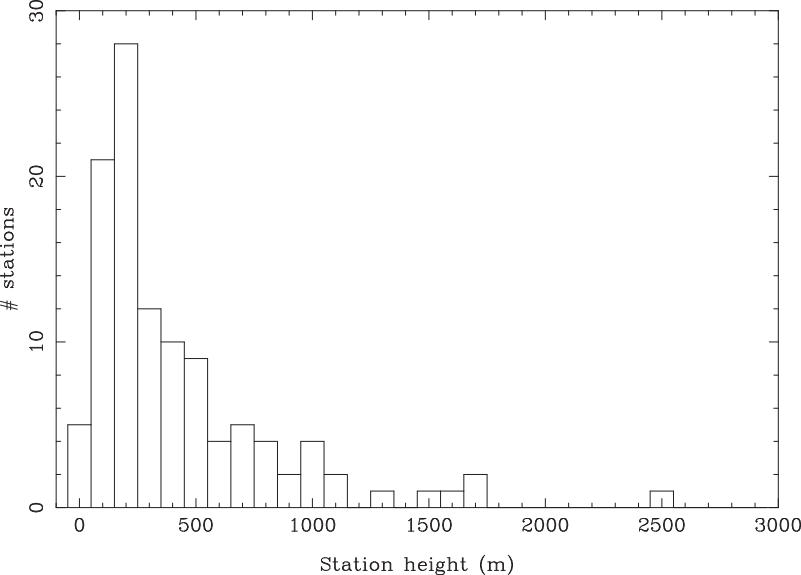
Figure 9. Top: Weather chart for 24 December 1999 at 12 UTC from the Royal Netherlands Meteorological Institute. Middle: Weather chart for 25 December 1999 at 00 UTC from <http://www.wetterzentrale.de>. Bottom: E-OBS daily mean sea level pressure grid for 24 December 1999. The contour lines (also from E-OBS) are shown in steps of 5 hPa rounded off to 5 and 10 hPa.

Figure 10. Top left: Weather chart for 28 February 2010 at 00 UTC from the Royal Netherlands Meteorological Institute. Top right: same for 28 February 2010 at 06 UTC. Middle left: same for 28 February 2010 at 12 UTC. Middle right: same for 28 February 2010 18 UTC. Bottom: E-OBS daily mean sea level pressure grid for 28 February 2010. The contour lines (also from E-OBS) are shown in steps of 5 hPa rounded off to 5 and 10 hPa.

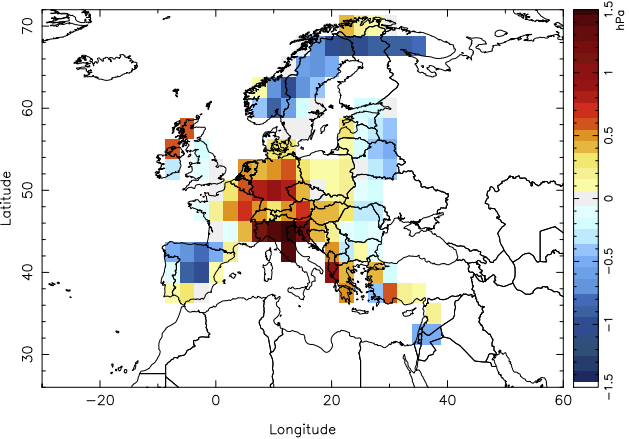




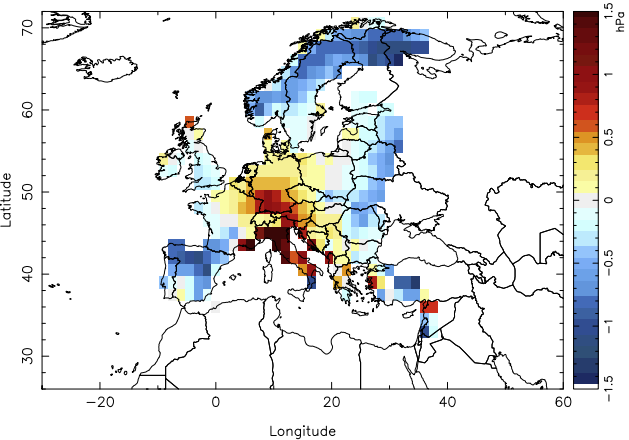




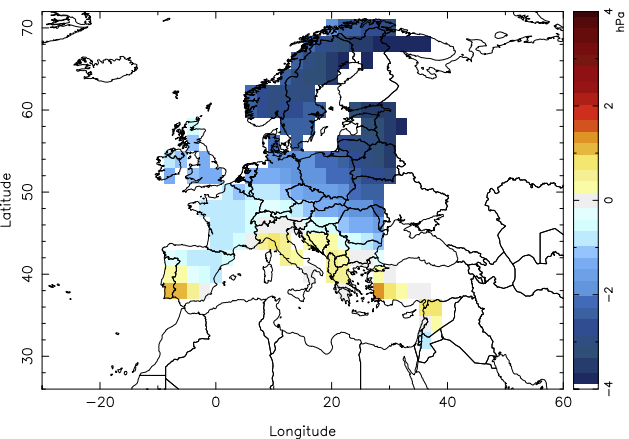
E-OBS - NCEP SLP-mean 1989-2001



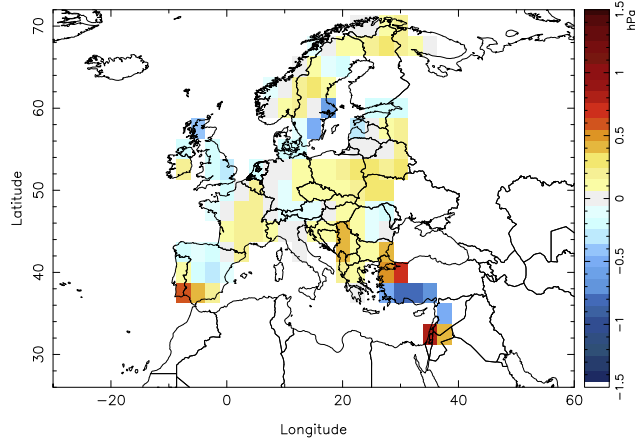
E-OBS - INTERIM SLP-mean 1989-2001



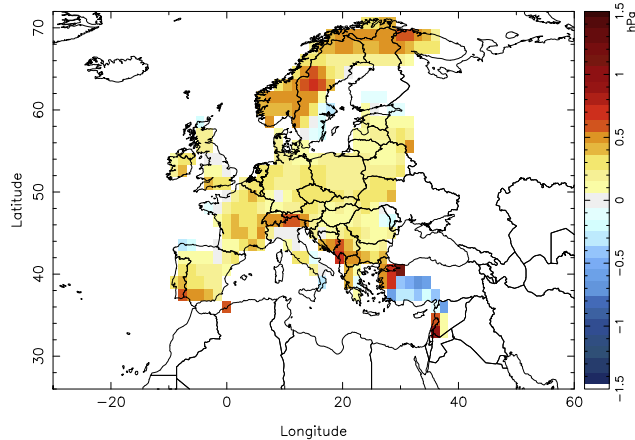
E-OBS - 20TH_CEN SLP-mean 1989-2001



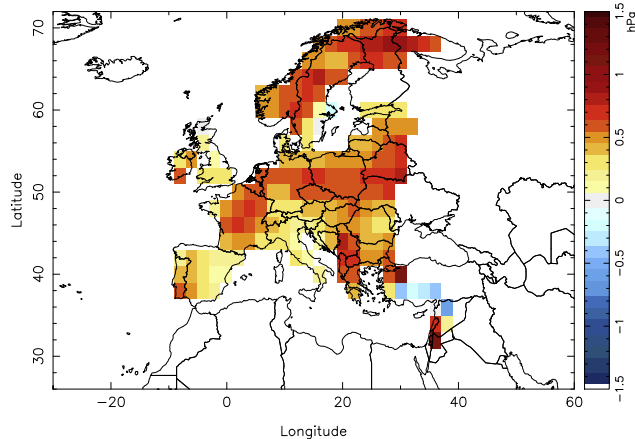
E-OBS - NCEP SLP-stdev 1989-2001



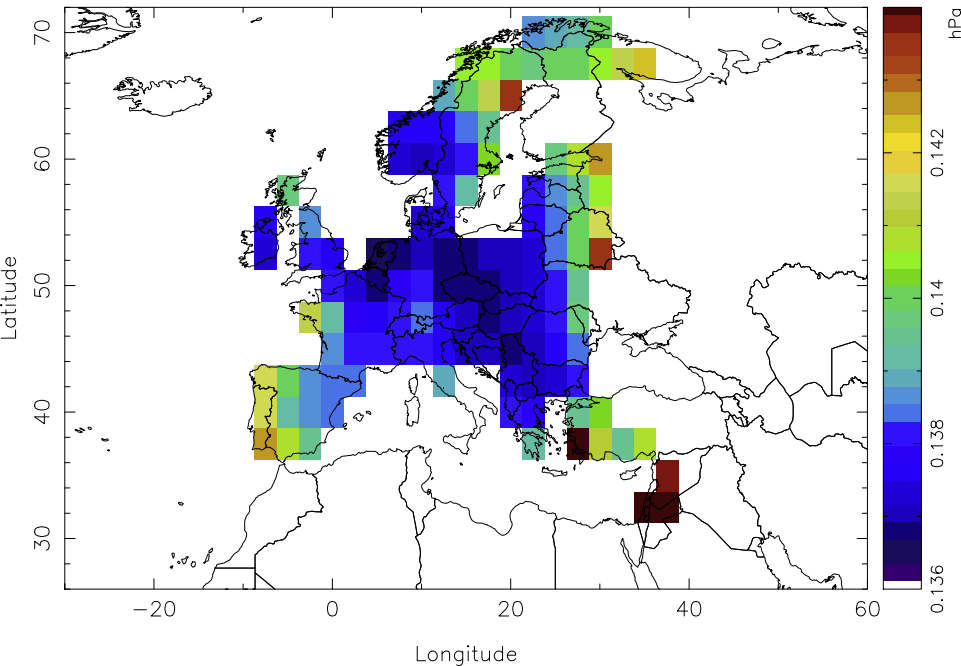
E-OBS - INTERIM SLP-stdev 1989-2001



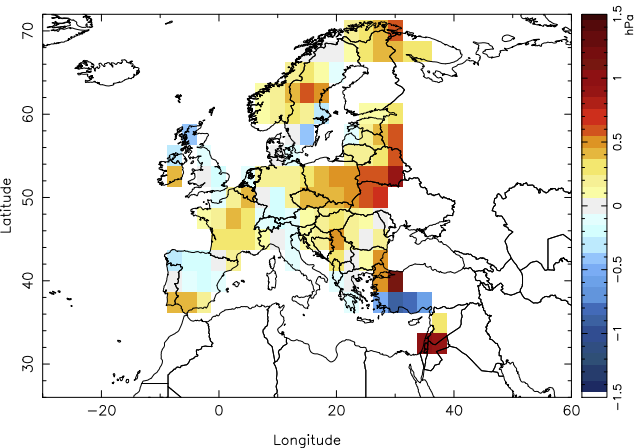
E-OBS - 20TH_CEN SLP-stdev 1989-2001



E-OBS SLP uncertainty 1989–2001



E-OBS - NCEP SLP-stdev 1989-2001 DJF



E-OBS - NCEP SLP-stdev 1989-2001 JJA

